Published in final edited form as:

J Biomech. 2017 January 04; 50: 42–49. doi:10.1016/j.jbiomech.2016.11.040.

Multi-component model of intramural hematoma

Martina Bukač[a] and **Mark Alber**[a,b,c,*]

[a]Department of Applied and Computational Mathematics and Statistics, University of Notre Dame, Notre Dame, IN 46556, USA

[b]Department of Medicine, Indiana University School of Medicine, Indianapolis, IN 46202, USA

[c]Department of Mathematics, University of California, Riverside, CA 92521, USA

Abstract

A novel multi-component model is introduced for studying interaction between blood flow and deforming aortic wall with intramural hematoma (IMH). The aortic wall is simulated by a composite structure submodel representing material properties of the three main wall layers. The IMH is described by a poroelasticity submodel which takes into account both the pressure inside hematoma and its deformation. The submodel of the hematoma is fully coupled with the aortic submodel as well as with the submodel of the pulsatile blood flow. Model simulations are used to investigate the relation between the peak wall stress, hematoma thickness and permeability in patients of different age. The results indicate that an increase in hematoma thickness leads to larger wall stress, which is in agreement with clinical data. Further simulations demonstrate that a hematoma with smaller permeability results in larger wall stress, suggesting that blood coagulation in hematoma might increase its mechanical stability. This is in agreement with previous experimental observations of coagulation having a beneficial effect on the condition of a patient with the IMH.

Keywords

Intramural hemorrhage; Finite element model; Poroelasticity; Flexible wall; Multi-component model

1. Introduction

Aortic dissection is a serious medical condition characterized by tearing of the inner layer of the aorta which results in blood surging through the tear causing the inner and middle layers of the aorta to separate. Rupture of the outside aortic wall of the blood-filled vessel often results in fatal aortic dissection. Aortic intramural hematoma (IMH) is an atypical form of

*Corresponding author. malber@nd.edu. Telephone number: (951) 827-3122. Fax: (951) 827-7314.

7. Conflict of interest statement

There is no conflict of interest.

aortic dissection. It results from the rupture of the vasa vasorum and formation of a hemorrhage in the aortic wall. Its distinguishing feature is an absence of the tear in the inner layer that characterizes classic aortic dissection. However, since the aortic wall weakens after formation of an IMH, the rupture within the wall might propagate and lead to dissection (Sawhney et al. (2001), Tsai et al. (2009)). An aortic IMH was found in 5–20% of patients who had shown signs of acute aortic syndromes. Improvement is observed in approximately 10% of patients, while progression to classic dissection occurs in 29–47% of patients and carries a risk of wall rupture in 20–45% of patients (Tsai et al. (2009)). Even though levels of morbidity and mortality due to IMH are as high as in case of classic dissection, the appropriate treatment of the IMH is neither well defined nor understood.

Mathematical modeling and numerical simulations have been recently used for predicting variety of patient specific health conditions which currently can not be determined based only on experimental data. In particular, numerical simulations have been used to determine stress distribution in the aortic wall under different conditions. For example, wall stress in an aorta with a growing aneurysm has been investigated by Thubrikar et al. (1999) as a possible mechanism for the development of transverse intimal tears in aortic dissections. A patient specific study was performed by Nathan et al. (2011) where local thoracic aortic wall stress was estimated using finite element analysis. The influence of the aortic root movement on the aortic wall stress was investigated by Beller et al. (2004) using a single layer model of the wall. The computed wall stress was used to explain why aortic dissection occured more often in this location. Stress distribution in each layer of the aorta was investigated by Gao et al. (2006a,b). However, since the aortic outlet zero pressure was applied, the effects of the downstream flow were not taken into account. A similar study was performed by Khanafer and Berguer (2009) with imposed physiologically relevant pressure values. A hemodynamics-based model was proposed by Menichini and Xu (2016) to study formation and growth of thrombus in the aortic dissection. The model was used for simulating different idealized aortic dissections to investigate the effect of geometric features of the aorta on thrombus formation.

A novel two-dimensional multi-component model is introduced in this paper for studying interaction between pulsatile blood flow and aortic wall with the IMH. The model describes dynamics of main three layers of the aortic wall and takes into account differences in their mechanical properties. In contrast with the previous studies, the model describes in detail the dynamics of the IMH and its interaction with the deformed aortic wall. The IMH is caused by the hemorrhage into the aortic wall, and the false lumen is known to cause formation of blood clots (Tsai et al. (2007)). Therefore, we assume that IMH consists of both fluid and solid phases. Hence, we describe the IMH using a poroelastic submodel capable of simulating how different distributions of the coagulated blood within IMH could influence its mechanical properties. The submodel for the aorta with IMH is coupled with the submodel for blood flow in the lumen. The coupling between blood flow and a 2-layer structure model was previously considered by Bukač et al. (2015), but without the presence of the poroelastic material. Furthermore, the coupling between the fluid, a single layer, thin elastic structure and poroelastic material was previously considered by Bukač (2016), but in a different configuration. The poroelastic material in Bukač (2016) was in contact with both

fluid and the thin elastic structure. In contrast with the previous work, in our present model the poroelastic submodel representing IMH is fully immersed in the 3-layer aortic wall.

Model simulations of the aortic blood flow under physiological conditions were performed using the finite element method. Finally, model simulations were used to investigate relation between the peak wall stress, hematoma thickness and permeability in patients of different age.

2. Methods

The multi-component model describes blood flow in a section of a descending aorta with the IMH (see Figure 1). Similar to the work by Khanafer and Berguer (2009), an idealized, axially symmetric section of an artery is considered. This assumption is justified by CT observations indicating that IMH often appears in the form of a focal region of a symmetric, homogeneous wall thickening (see Figure 2). Moreover, cross section images show that the IMH maintains a constant circumferential relationship with the aortic wall (Rajiah (2013), Herlinger et al. (2001), Nienaber et al. (1995), Kazerooni and Gross (2004)).

2.1. Blood flow

Blood is a mixture of plasma, red and white blood cells, proteins, lipoproteins and ions, and hence it is not homogeneous or Newtonian. However, in medium-to-large vessels, the size of individual elements becomes negligible with respect to the blood vessel diameter, and the Navier-Stokes equations for an incompressible, viscous fluid have been extensively used for simulations (Nakamura et al. (2006), Vasava et al. (2012), Sankaran et al. (2012)):

$$\rho_f\,(\partial_t \boldsymbol{v} + \boldsymbol{v}\cdot\nabla\boldsymbol{v}) = \nabla\cdot\boldsymbol{\sigma}^f, \quad (1)$$

$$\nabla\cdot\boldsymbol{v} = 0, \quad (2)$$

where $\boldsymbol{v}$ is the velocity, $\boldsymbol{\sigma}^f = -p_f\boldsymbol{I} + 2\mu_f\boldsymbol{D}(\boldsymbol{v})$ is the fluid stress tensor, p_f is the fluid pressure, ρ_f is the fluid density, μ_f is the fluid viscosity and $\boldsymbol{D}(\boldsymbol{v}) = (\nabla\boldsymbol{v} + (\nabla\boldsymbol{v})^T)/2$ is the strain rate tensor. At the beginning of the simulation, the fluid domain is defined as a rectangle of length L = 10 cm and height R_{lumen} = 1 cm, where the height is the vessel radius. This is consistent with the experimental measurements of the aortic diameters reported by Wolak et al. (2008) and O'Rourke and Nichols (2005). The blood density is taken to be ρ_f = 1 g/cm^3 and viscosity μ_f = 0.035 g/cm s. We impose symmetry boundary conditions at the fluid bottom boundary Γ_b^f (see Figure 1) (Khanafer and Berguer (2009), Bukač et al. (2015)).

A physiological, pulsatile velocity $v_D(t)$ is imposed at the inlet of the fluid domain Γ_{in}^f, while a pressure waveform $p_{out}(t)$ is imposed at the outlet Γ_{out}^f see Figure 3) (Mills et al. (1970)). The boundary conditions are implemented in the following way:

$$\boldsymbol{v}=\left(v_D(t)\frac{R_{lumen}^2-r^2}{R_{lumen}^2},0\right) \quad \text{on } \Gamma_{in}^f\times(0,T), \tag{3}$$

$$\boldsymbol{\sigma}^f\boldsymbol{n}^f=-p_{out}(t)\boldsymbol{n}^f \quad \text{on } \Gamma_{out}^f\times(0,T), \tag{4}$$

where $\boldsymbol{n}^f$ denotes the outward normals to the fluid boundary.

The velocity waveform v_D corresponds to the Reynolds number of 1200, in which case the flow can be categorized as laminar (Stokes (1851), Holman (2001)). To circumvent the issues related to the motion of the fluid domain due to the fluid-structure interaction, we use the Navier-Stokes equations in the ALE form (Donea (1983), Duarte et al. (2004), Bukač et al. (2015)).

2.2. Aortic wall

Aortic walls are represented as a composite material consisting of three main layers: tunica intima, media and adventitia. We model the aortic wall using a composite structure model, taking into account mechanical properties of each layer. Average thickness ratio of intima/media/adventitia was shown to be 13/56/31 (Schulze-Bauer et al. (2003)). Hence, we model the intimal layer as a thin, elastic structure using the Koiter shell model (Bukač et al. (2013))

$$\rho_i h_i\partial_{tt}\eta_z^i-\frac{h_iE_i}{1-\sigma_i^2}\partial_{zz}\eta_z^i-\frac{h_i}{R_i}\frac{E_i\sigma_i}{1-\sigma_i^2}\partial_z\eta_r^i=f_z^i \tag{5}$$

$$\rho_i h_i\partial_{tt}\eta_r^i+\frac{h_iE_i}{R_i^2(1-\sigma_i^2)}\left(1+\frac{h_i^2}{12R_i^2}\right)\eta_r^i-\frac{h_i^3}{6}\frac{E_i\sigma_i}{R_i^2(1-\sigma_i^2)}\partial_{zz}\eta_r^i+\frac{h_i}{R_i}\frac{E_i\sigma_i}{1-\sigma_i^2}\partial_z\eta_z^i=f_r^i. \tag{6}$$

The intimal displacement is denoted by $\boldsymbol{\eta}^i=(\eta_z^i,\eta_r^i)$, where η_z^i denotes the longitudinal and η_r^i the radial displacement. The intimal density is denoted by $\boldsymbol{\rho_i}$, the thickness by h_i, and the force applied to the wall by $\boldsymbol{f_i}$. The parameters E_i and σ_i are the Young's modulus and the Poisson's ratio of the intimal layer, respectively.

The deformation of the media/adventitia complex is modeled using the 2D equations of linear elasticity (Quaini (2009), Bukač et al. (2015)):

$$\rho_{ma}\partial_{tt}\boldsymbol{\eta}^{ma}=\nabla\cdot\boldsymbol{\sigma}^s, \tag{7}$$

where $\boldsymbol{\eta}^{ma}$ is the structure displacement and ρ_{ma} is the density. One of the common simplifying assumptions in models of blood flow interaction with the vessel wall is

treatment of the biomechanical material properties of the vessel as linearly elastic, homogeneous material (Thubrikar et al. (2001), Hua and Mower (2001), Scotti et al. (2005), Giannoglou et al. (2006)). Some authors even claim that although human arterial tissue acts like a non-linear material, at pressures above 80 mmHg (10.67 KPa) the aorta behaves more like a linearly elastic material (Giannoglou et al. (2006), Thubrikar et al. (2001)). Hence, we assume that arterial wall behaves as isotropic, linearly elastic Saint-Venant Kirchhoff material. Thus,

$$\boldsymbol{\sigma}^s = \frac{E_{ma}}{1+\sigma_{ma}}\boldsymbol{D}(\boldsymbol{\eta}^{ma}) + \frac{E_{ma}\sigma_{ma}}{(1+\sigma_{ma})(1-2\sigma_{ma})}(\nabla\cdot\boldsymbol{\eta}^{ma})\boldsymbol{I},$$

where E_{ma} and σ_{ma} are the Young's modulus and the Poisson's ratio, respectively.

Based on the experimental measurements from Xie et al. (1995) and Fischer et al. (2002), we assume that the Young's moduli of the intima, media and adventitia are, 2, 6 and 4 MPa, respectively. Poisson's ratio of all three layers is set to 0.45 (Khanafer and Berguer (2009)). Thicknesses of intima, media and adventitia are 0.04 cm, 0.12 cm and 0.06 cm, respectively. The total aortic wall thickness is 0.22 cm, in agreement with the experimental measurements in Malayeri et al. (2008) and Alimohammadi et al. (2016). Furthermore, the density of all three layers is set to 1.1 g/cm^3. The aortic wall is assumed to be fixed at the inlet and outlet boundaries. The adventitia is exposed at the external boundary to zero external ambient pressure. We assume the continuity of the displacement and the conservation of momentum between the three layers.

2.3. Intramural hematoma

One of the novel features of the model described in this paper is that we account for the pressure inside the IMH and its deformation. The IMH is located in the medial layer. It has been observed using echocardiography that the hemorrhage has a thrombus-like, homogeneous echo structure in some patients, while in others it has small echo-free areas probably representing contained liquid zones (Nienaber et al. (1995), Tsai et al. (2007), Mohr-Kahaly et al. (1994)). Hence, we model the IMH as a fully saturated poroelastic material. In this way we take into account the fluid pressure inside the IMH created by the hemorrhage, as well as the deformation of the IMH due to the movement of the aortic wall. The level of thrombosis is related to the permeability of the IMH. Even though we assume that there is no flow coming inside or outside the IMH, the permeability of the region will affect its mechanical properties.

We model the IMH using the Biot's poroelasticity model (Chen (1994)). The pressure and the deformation are mutually dependent and fully coupled in Biot's model. The model is given as follows:

$$\rho_h \partial_{tt}\boldsymbol{U} = \nabla\cdot\boldsymbol{\sigma}^h, \quad (8)$$

$$\alpha\nabla\cdot(\partial_t \boldsymbol{U})-\nabla\cdot(\boldsymbol{\kappa}\nabla p_p)=0, \quad (9)$$

where $\boldsymbol{U}$ is the displacement p_p is the fluid pressure. The stress tensor of the poroelastic medium is given by $\boldsymbol{\sigma}^h = \boldsymbol{\sigma}^E(\boldsymbol{U}) - \alpha p_p \boldsymbol{I}$, where $\boldsymbol{\sigma}^E(\boldsymbol{U})$ denotes the elasticity stress tensor. For the Saint Vernant-Kirchoff elastic material,

$$\boldsymbol{\sigma}^E(\boldsymbol{U})=\frac{E_h}{1+\sigma_h}\boldsymbol{D}(\boldsymbol{U})+\frac{E_h\sigma_h}{(1+\sigma_h)(1-2\sigma_h)}(\nabla\cdot\boldsymbol{U})\boldsymbol{I},$$

where E_h and σ_h are the Young's modulus and the Poisson's ratio, respectively. The density of the solid material is denotes by ρ_h and the permeability tensor by $\boldsymbol{\kappa}$. Finally, α is the Biot parameter accounting for the coupling strength between the fluid and the solid phase in the two-phase material.

In the numerical simulations, we used the value of $\rho_h = 1.3$ g/cm^3. IMH is a region filled with clotted blood. Since there are no experimental measurements of material properties of IMH, we estimate its permeability using measurements of the permeability of different blood clots. We used permeability values varying from the values for clotted blood with higher permeability and for less permeable blood clots, to values close to the permeability of the aortic wall.

Furthermore, we assume the following mechanical properties of the IMH: $E_h = 5 \cdot 10^7$ dyne/cm^2 and $\sigma_h = 0.49$ obtained from the experimental measurements of blood clots reported in Kim et al. (2015). Finally, we assume that $\alpha = 1$. Specific values of permeability are provided in the Results section.

2.4. Coupling of the sub-models of the blood flow, vessel walls and thrombus

The interaction of arterial walls with the blood flow plays a crucial role in the normal physiology and pathophysiology of the human cardiovascular system. The coupling between the blood and aortic walls is described in our model as follows (Bukač et al. (2015), Bukač (2016)):

$$\text{The continuity of velocities:} \quad \boldsymbol{v}=\partial_t \boldsymbol{\eta}^i, \quad (10)$$

$$\text{The conservation of momentum:} \quad -\boldsymbol{\sigma}^f \boldsymbol{n}^f - \boldsymbol{\sigma}^s \boldsymbol{n}^s = \boldsymbol{f}^i, \quad (11)$$

where $\boldsymbol{n}^s$ is the outward normal to the aortic wall.

Aortic walls are in contact with the IMH. Denote by $\boldsymbol{n}^h$ the outward normal to the IMH. The coupling conditions at the IMH-aortic wall interface are given as follows (Bukač (2016)):

$$\text{no relative mass flux:} \quad \boldsymbol{\kappa}\nabla p_p \cdot \boldsymbol{n}^h = 0, \tag{12}$$

$$\text{continuity of the displacement:} \quad \boldsymbol{U} = \boldsymbol{\eta}_m, \tag{13}$$

$$\text{balance of contact forces:} \quad \boldsymbol{\sigma}^s \boldsymbol{n}^s = -\boldsymbol{\sigma}^h \boldsymbol{n}^h. \tag{14}$$

Complete model system of coupled equations has the following form.

$$\rho_f \left(\partial_t \boldsymbol{v} + \boldsymbol{v} \cdot \nabla \boldsymbol{v}\right) = \nabla \cdot \boldsymbol{\sigma}^f, \quad \nabla \cdot \boldsymbol{v} = 0, \tag{15}$$

$$\rho_i h_i \partial_{tt} \eta_z^i - \frac{h_i E_i}{1-\sigma_i^2} \partial_{zz} \eta_z^i - \frac{h_i}{R_i} \frac{E_i \sigma_i}{1-\sigma_i^2} \partial_z \eta_r^i = f_z^i \tag{16}$$

$$\rho_i h_i \partial_{tt} \eta_r^i + \frac{h_i E_i}{R_i^2 (1-\sigma_i^2)} \left(1 + \frac{h_i^2}{12 R_i^2}\right) \eta_r^i - \frac{h_i^3}{6} \frac{E_i \sigma_i}{R_i^2 (1-\sigma_i^2)} \partial_{zz} \quad \eta_r^i + \frac{h_i}{R_i} \frac{E_i \sigma_i}{1-\sigma_i^2} \partial_z \eta_z^i = f_r^i, \tag{17}$$

$$\rho_{ma} \partial_{tt} \boldsymbol{\eta}^{ma} = \nabla \cdot \boldsymbol{\sigma}^s, \tag{18}$$

$$\rho_h \partial_{tt} \boldsymbol{U} = \nabla \cdot \boldsymbol{\sigma}^h, \quad \alpha \nabla \cdot (\partial_t \boldsymbol{U}) - \nabla \cdot (\boldsymbol{\kappa} \nabla p_p) = 0, \tag{19}$$

$$\boldsymbol{v} = \partial_t \boldsymbol{\eta}^i, \quad -\boldsymbol{\sigma}^f \boldsymbol{n}^f - \boldsymbol{\sigma}^s \boldsymbol{n}^s = \boldsymbol{f}^i, \tag{20}$$

$$\boldsymbol{\kappa} \nabla p_p \cdot \boldsymbol{n}^h = 0, \quad \boldsymbol{U} = \boldsymbol{\eta}_m, \quad \boldsymbol{\sigma}^s \boldsymbol{n}^s = -\boldsymbol{\sigma}^h \boldsymbol{n}^h. \tag{21}$$

The system consists of fluid submodel (1)–(2), elastic structure submodel (5)–(7) and poroelastic material submodel (8)–(9), subject to coupling conditions (10)–(14).

2.5. Numerical scheme

The coupled problem features different physical phenomena defined on separate domains. Hence, we solve the full problem using a partitioned approach so that the fluid dynamics of blood flow are solved separately from the aortic wall and IMH mechanics. To separate the fluid sub-problem from the composite structure sub-problem describing the aortic wall, we use a stable, partitioned, non-iterative scheme called the kinematically coupled β scheme, presented and analyzed by Bukač et al. (2015) and Bukač and Muha (2016). It was shown in Bukač and Muha (2016) that the scheme is unconditionally stable and first-order accurate in time. The aortic wall and IMH mechanics are solved together, in a monolithic fashion.

3. Hemodynamics analysis

The growth of the IMH might cause an intimal tear leading to the classic aortic dissection. The occurrence of the intimal tear is associated with the increase of the stress acting on the wall, which exceeds the mechanical failure strength of the wall. The Peak Wall Stress (PWS) is often used to quantify the risk of the vessel wall rupture (Polzer et al. (2012), Khanafer and Berguer (2009), Venkatasubramaniam et al. (2004)). The PWS is defined as the maximum von Mises stress ($PWS = \max \sigma_{VM}$) in the vessel wall, where

$$\sigma_{VM} = \sqrt{\sigma_1^2 - \sigma_1\sigma_2 + \sigma_2^2}, \quad (22)$$

and σ_1 and σ_2 are principal stresses in the wall.

The objective of this paper is to quantify the risk factors which might lead to progression of the disease and wall rupture, manifested by the increase of the PWS. We studied dependance of the von Mises stress on the IMH thickness, IMH permeability and patient age. We also performed numerical simulations for the an aorta without IMH in order to compare our results with the outcome for a healthy patient. In the simulations for a healthy patient, we assumed that there was no IMH present in the wall, while the mechanical properties of the wall remained the same.

To obtain a good resolution of the solution based on the assumed value of the Reynolds number of 2400, we used 20746 nodes in the fluid domain, 6372 nodes in the aortic wall domain and 15057 nodes in the domain representing IMH. Mesh and time step independence tests were preformed. Linear systems corresponding to each subproblem were solved using the parallel solver MUMPS. The time step used in the simulations was $\Delta t = 10^{-4}$ s. The final results were obtained after periodic regime was achieved after 3 cardiac cycles.

4. Results

4.1. Effects of the IMH thickness

In this section, we perform a computational study to quantify the effects of the IMH thickness on the von Mises stress in the aortic wall. The normal aortic thickness is less than

0.3 cm by any imaging modality. Hence it is believed that the aortic wall thickness larger than 0.5 cm implies the diagnosis of IMH in patients with typical clinical symptoms suggesting acute aortic syndrome (Song (2004)), while the maximum IMH thickness is often even larger than 1 cm (Choi et al. (2014), Evangelista et al. (2004)).

We considered IMHs of thicknesses 0.6, 0.8 and 1.0 cm. In all three cases we use the value of the IMH permeability $\boldsymbol{\kappa} = 10^{-10}\boldsymbol{I}$ cm^3 s/g. The permeability is taken from the measurements of intramural thrombi reported by Polzer et al. (2012).

Figure 4 shows the comparison of the velocity and pressure in the lumen over one cardiac cycle obtained in the case of a healthy aorta and aortas with IMH, for IMH thicknesses 0.6, 0.8 and 1.0 cm. The values of the velocity and pressure are taken from the center of the domain, i.e. point (5, 0). There are no significant differences in the velocity between the healthy aorta and the diseased aortas with IMH of thicknesses 0.6 and 0.8 cm. However, the peak and mean velocity in the case of IMH with thickness 1.0 cm is 9% and 33% larger, respectively, than in the healthy case. In all three IMH cases, we do not observe differences in the luminal pressure when compared to the healthy case.

The displacements of the intimal and adventitial region at the center of the wall ($x = 5$ cm), in healthy and diseased cases, are shown in Figure 5. The aortic diameter ranges from 2.19 cm to 2.29 cm, which agrees well with the displacement measured *in vivo* by Stefanadis et al. (1995), see Figure 7, right panel in (Stefanadis et al. (1995)). Displacements in the diseased cases are larger than the displacement in the healthy case in both regions of the aortic wall. The average displacement over one cardiac cycle in a diseased aorta is by 5% larger than in the healthy case, while the peak displacement is increased by 6%. There are no significant differences in the displacement of aortas with IMH for different values of the IMH thickness.

The propagation of the IMH and the occurrence of the intimal tear is associated with the increased values of the PWS defined in (22). In all three cases of the aortas with IMH, the PWS occurred in the media/intima region below the IMH. The PWS in the case when the IMH thickness is 1.0 cm is shown in the left panel of Figure 6.

The comparison of PWS in aortas with IMH of different thicknesses is shown in the right panel of Figure 6. We observe that the PWS increases with the increase of the IMH thickness. Hence, the risk of rupture of the IMH is greater in aortas with thicker IMH. This is consistent with experimental observations by Song (2004).

4.2. Effects of the IMH permeability

In this section we quantify the effects of the permeability of the IMH on the risk of disease propagation and wall rupture, associated with the higher values of the PWS. We perform the numerical simulations for a diseased aorta with IMH thickness 1.0 cm using values of permeability $\boldsymbol{\kappa} = 10^{-8}\boldsymbol{I}$, $10^{-10}\boldsymbol{I}$ and $10^{-12}\boldsymbol{I}$ cm^3 s/g.

The left panel in Figure 7 shows the comparison of the velocity in the center of the fluid domain over one cardiac cycle obtained in the case of a healthy aorta and diseased aortas

with different values of IMH permeability. In all cases, aortas with IMH exhibit an increase in the fluid velocity. The peak fluid velocity is 9% larger then in the healthy case, while the mean velocity is increased by 33%. As in the previous section, we did not observe any differences in the pressure.

The displacement in the intimal region, in the healthy and the diseased cases, is shown in the right panel in Figure 7. Similar behavior as in the previous section is observed in this case. The average displacement at the center of the vessel is increased by 5% in the diseased cases in both intima and adventitia. The peak displacement is increased by 6% in the diseased aortas. There are no significant differences in the displacement of aortas with IMH for different values of the IMH permeability.

Finally, we investigate the relationship between the permeability of the IMH region and the PWS in the aortic wall. The PWS for different values of the permeability is achieved at the same location as shown in Figure 6. The PWS at that location, over one cardiac cycle, for different values of permeability is shown in Figure 8. We can see that the IMH with smaller permeability causes smaller PWS. The PWS is the largest for $\boldsymbol{\kappa} = 10^{-8}\boldsymbol{I}$ cm^3 s/g. As the permeability decreases to $\boldsymbol{\kappa} = 10^{-12}\boldsymbol{I}$ cm^3 s/g, the PWS drops by 3%.

4.3. Effects of age

The aortic diameter increases with age. The normal expansion rate is about 1–2 mm/year. The aging of the aorta is accompanied by an increase in wall stiffness and thickness, caused by the structural changes including an increase in the collagen content. The effects of these changes on the blood flow in a healthy and diseased aortas are studied in this section. We assume that the aortic diameter of a heathy, older person is 2.4 cm (Erbel and Eggebrecht (2006)). Thicknesses of intima, media and adventitia are 0.5 cm, 1.4 cm and 0.6 cm, respectively, resulting in 2.5 cm total wall thickness. Measurements by Wuyts et al. (1995), Learoyd and Taylor (1966) indicate that the arterial stiffness doubles in older people. Hence, we assume that the Young's moduli are 4, 12 an 8 MPa for intima, media and adventitia, respectively.

Our simulations showed that velocity in the lumen in a healthy older person is higher by 10% then in a healthy younger person. This agrees well with the measurements reported by Erbel and Eggebrecht (2006) and provided calibration for our model. We also did not observe major difference between the pressure in a younger and older healthy person.

The left panel in Figure 9 shows a comparison between the intimal displacement in an old, healthy aorta and old aortas with IMHs of thicknesses 0.6, 0.8 and 1.0 cm. The permeability in all cases is $10^{-10}\boldsymbol{I}$ cm^3 s/g. The maximum displacement is about 20% larger in all cases with IMH than in the healthy case. However, there are no differences between the displacements in cases with IMH with different IMH thicknesses.

The right panel in Figure 9 shows comparison of the intimal displacement in a healthy older people and older people with IMHs of permeabilities 10^{-8} and $10^{-10}\boldsymbol{I}$ cm^3 s/g. The IMH thickness in all three cases is 0.8 cm. We observe that in both cases with IMH, the

displacement is larger than in the healthy case. Furthermore, in cases with IMH the displacement is larger for smaller value of the permeability.

Finally, the relation between PWS and IMH thickness and permeability is shown in Figure 10. The left panel shows the PWS obtained for three different valued of IMH thickness, where the permeability in all cases is $\boldsymbol{\kappa} = 10^{-10}\boldsymbol{I}$ cm^3 s/g. Our results show that, as expected, the PWS increases as the IMH thickness increases. The right panel shows the PWS obtained for different values of permeability and the same IMH thickness of 1.0 cm. Notice that the PWS is larger for larger values of permeability. We also note that PWS is larger in older patients then young patients (see Figure 8). Moreover, the difference in PWS with respect to IMH permeability is more significant in older patients. The increased PWS in older people is due to the combination of age related hemodynamical changes. Besides the increased stiffness and thickness of the aortic wall, these changes include the increase in the aortic diameter, causing higher blood velocity (increased by 10% in comparison with a young person), and a slight increase in peak systolic pressure causing an increase in the wall stress.

5. Discussion

A novel multi-component model is presented in this paper for simulating blood flow in an aorta with realistic representation of an IMH formed in the aortic wall. The model captures both deformation of the IMH and pressure inside it. There are no experimental measurements of the material properties of different parts of the IMH available at this time. Hence, to estimate the permeability of different parts of the IMH we used the permeability values ranging from the values for clotted blood with higher permeability and for less permeable blood clots, to values close to the permeability of the aortic wall.

Simulations were preformed for studying blood flow in aortas in young and old patients with IMH. Results in Figures 8 and 10 indicate that IMH regions with higher permeability (with smaller amounts of coagulated blood) have higher PWS than the same domains with smaller permeability in both young and old individuals. Furthermore, the difference between PWS obtained using different IMH permeabilities is much more pronounced in older people. Hence, increased blood coagulation in the IMH, which determines permeability, might lead to more stable IMH. This is in agreement with previous experimental observations (Menichini and Xu (2016)) of coagulation having beneficial effect on patient condition.

Since our model captures both pressure inside the IMH and its deformation, it could be extended for modeling the IMH progression into the classical dissection in the form of the pressure driven crack propagating in an elastic material. To capture this process, the model presented in this paper needs to be coupled with a phase field submodel of the propagating fractures. This will be implemented in our future work. Furthermore, we will extend our description of the vessel wall by developing a more realistic non-linear model for anisotropic solids. We are also working on a 3D extension of the model and incorporating patient specific aorta geometries.

Acknowledgments

This research was supported by the NIH grant 1U01HL116330, NSF DMS grant 1318763 and NSF DMS grant 1619993.

References

Alimohammadi M, Pichardo-Almarza C, Agu O, Díaz-Zuccarini V. Development of a patient-specific multi-scale model to understand atherosclerosis and calcification locations: Comparison with in vivo data in an aortic dissection. Frontiers in Physiology. 2016; 7:238. [PubMed: 27445834]

Beller C, Labrosse M, Thubrikar M, Robicsek F. Role of aortic root motion in the pathogenesis of aortic dissection. Circulation. 2004; 109:763–769. [PubMed: 14970113]

Bukač M. A loosely-coupled scheme for the interaction between a fluid, elastic structure and poroelastic material. Journal of Computational Physics. 2016; 313:377–399.

Bukač M, Čanić S, Glowinski R, Tambača J, Quaini A. Fluid-structure interaction in blood flow capturing non-zero longitudinal structure displacement. Journal of Computational Physics. 2013; 235:515–541.

Bukač M, Muha B. Stability and convergence analysis of the extensions of the kinematically coupled scheme for the fluid-structure interaction. SIAM Journal on Numerical Analysis. 2016; 54:3032–3061.

Bukač M, Čanić S, Muha B. A partitioned scheme for fluid-composite structure interaction problems. Journal of Computational Physics. 2015; 281:493–517.

Chen J. Time domain fundamental solution to Biot's complete equations of dynamic poroelasticity. Part II: Three-dimensional solution. International Journal of Solids and Structures. 1994; 31:169–202.

Choi YJ, Son JW, Lee SH, Kim U, Shin DG, Kim YJ, Hur SH, Nam CW, Cho YK, Lee BR, et al. Treatment patterns and their outcomes of acute aortic intramural hematoma in real world: multicenter registry for aortic intramural hematoma. BMC cardiovascular disorders. 2014; 14:1. [PubMed: 24400643]

Donea, J. Computational methods for transient analysis. North-Holland; Amsterdam: 1983. Arbitrary Lagrangian-Eulerian finite element methods.

Duarte F, Gormaz R, Natesan S. Arbitrary Lagrangian-Eulerian method for Navier-Stokes equations with moving boundaries. Computer Methods in Applied Mechanics and Engineering. 2004; 193:4819–4836.

Erbel R, Eggebrecht H. Aortic dimensions and the risk of dissection. Heart. 2006; 92:137–142. [PubMed: 16365370]

Evangelista A, Dominguez R, Sebastia C, Salas A, Permanyer-Miralda G, Avegliano G, Gomez-Bosh Z, Gonzalez-Alujas T, del Castillo HG, Soler-Soler J. Prognostic value of clinical and morphologic findings in short-term evolution of aortic intramural haematoma. European Heart Journal. 2004; 25:81–87. [PubMed: 14683746]

Fischer EC, Armentano R, Pessana F, Graf S, Romero L, Christen A, Simon A, Levenson J. Endothelium-dependent arterial wall tone elasticity modulated by blood viscosity. American Journal of Physiology-Heart and Circulatory Physiology. 2002; 282:H389–H394. [PubMed: 11788384]

Gao F, Guo Z, Sakamoto M, Matsuzawa T. Fluid-structure interaction within a layered aortic arch model. Journal of biological physics. 2006a; 32:435–454. [PubMed: 19669449]

Gao F, Watanabe M, Matsuzawa T, et al. Stress analysis in a layered aortic arch model under pulsatile blood flow. Biomed Eng Online. 2006b; 5:1–11.

Giannoglou G, Giannakoulas G, Soulis J, Chatzizisis Y, Perdikides T, Melas N, Parcharidis G, Louridas G. Predicting the risk of rupture of abdominal aortic aneurysms by utilizing various geometrical parameters: revisiting the diameter criterion. Angiology. 2006; 57:487–494. [PubMed: 17022385]

Herlinger, H.; Maglinte, D.; Birnbaum, B. Clinical imaging of the small intestine. Springer Science & Business Media; 2001.

Holman, JP. Heat transfer. 2001. Eighth SI Metric Edition

Hua J, Mower WR. Simple geometric characteristics fail to reliably predict abdominal aortic aneurysm wall stresses. Journal of vascular surgery. 2001; 34:308–315. [PubMed: 11496284]

Kazerooni, E.; Gross, B. Cardiopulmonary imaging. Vol. 4. Lippincott Williams & Wilkins; 2004.

Khanafer K, Berguer R. Fluid–structure interaction analysis of turbulent pulsatile flow within a layered aortic wall as related to aortic dissection. Journal of biomechanics. 2009; 42:2642–2648. [PubMed: 19765711]

Kim O, Liang X, Litvinov R, Weisel J, Alber M, Purohit P. Foam-like compression behavior of fibrin networks. Biomechanics and modeling in mechanobiology. 2015:1–16. [PubMed: 24718853]

Learoyd B, Taylor M. Alterations with age in the viscoelastic properties of human arterial walls. Circulation research. 1966; 18:278–292. [PubMed: 5904318]

Malayeri A, Natori S, Bahrami H, Bertoni A, Kronmal R, Lima J, Bluemke D. Relation of aortic wall thickness and distensibility to cardiovascular risk factors (from the Multi-Ethnic Study of Atherosclerosis [MESA]). The American journal of cardiology. 2008; 102:491–496. [PubMed: 18678312]

Masip A. Natural history and therapeutic management of acute aortic syndrome. Revista Española de Cardiología (English Edition). 2004; 57:667–679.

Menichini C, Xu XY. Mathematical modeling of thrombus formation in idealized models of aortic dissection: initial findings and potential applications. Journal of mathematical biology. 2016:1–22.

Mills C, Gabe I, Gault J, Mason D, Ross J, Braunwald E, Shillingford J. Pressure-flow relationships and vascular impedance in man. Cardiovasc Res. 1970; 4:405–417. [PubMed: 5533085]

Mohr-Kahaly S, Epbel R, Kearney P, Puth M, Meyer J. Aortic intramural hemorrhage visualized by transesophageal echocardiography: findings and prognostic implication. Journal of the American College of Cardiology. 1994; 23:658–664. [PubMed: 8113549]

Nakamura M, Wada S, Yamaguchi T. Computational analysis of blood flow in an integrated model of the left ventricle and the aorta. Journal of Biomechanical Engineering. 2006; 128:837–843. [PubMed: 17154683]

Nathan D, Xu C, Gorman J, Fairman R, Bavaria J, Gorman R, Chandran K, Jackson B. Pathogenesis of acute aortic dissection: a finite element stress analysis. The Annals of thoracic surgery. 2011; 91:458–463. [PubMed: 21256291]

Nienaber C, von Kodolitsch Y, Petersen B, Loose R, Helmchen U, Haverich A, Spiel-mann R. Intramural hemorrhage of the thoracic aorta diagnostic and therapeutic implications. Circulation. 1995; 92:1465–1472. [PubMed: 7664428]

O'Rourke M, Nichols W. Aortic diameter, aortic stiffness, and wave reflection increase with age and isolated systolic hypertension. Hypertension. 2005; 45:652–658. [PubMed: 15699456]

Polzer S, Gasser TC, Markert B, Bursa J, Skacel P. Impact of poroelasticity of intraluminal thrombus on wall stress of abdominal aortic aneurysms. BioMedical Eng. 2012

Quaini, A. PhD thesis. EPFL; Switzerland: 2009. Algorithms for fluid-structure interaction problems arising in hemodynamics.

Rajiah P. CT and MRI in the Evaluation of Thoracic Aortic Diseases. International journal of vascular medicine 2013. 2013

Sankaran S, Moghadam M, Kahn A, Tseng E, Guccione J, Marsden A. Patient-specific multiscale modeling of blood flow for coronary artery bypass graft surgery. Annals of biomedical engineering. 2012; 40:2228–2242. [PubMed: 22539149]

Sawhney N, DeMaria A, Blanchard D. Aortic intramural hematoma: an increasingly recognized and potentially fatal entity. Chest Journal. 2001; 120:1340–1346.

Schulze-Bauer C, Mrth C, Holzapfel G. Passive biaxial mechanical response of aged human iliac arteries. Journal of biomechanical engineering. 2003; 125:395–406. [PubMed: 12929245]

Scotti CM, Shkolnik AD, Muluk SC, Finol EA. Fluid-structure interaction in abdominal aortic aneurysms: effects of asymmetry and wall thickness. Biomedical engineering online. 2005; 4:1. [PubMed: 15631635]

Song J. Diagnosis of aortic intramural haematoma. Heart. 2004; 90:368–371. [PubMed: 15020502]

Stefanadis C, Stratos C, Vlachopoulos C, Marakas S, Boudoulas H, Kallikazaros I, Tsiamis E, Toutouzas K, Sioros L, Toutouzas P. Pressure-diameter relation of the human aorta a new method of determination by the application of a special ultrasonic dimension catheter. Circulation. 1995; 92:2210–2219. [PubMed: 7554204]

Stokes, G. On the effect of the internal friction of fluids on the motion of pendulums. Vol. 9. Pitt Press; 1851.

Thubrikar M, Agali P, Robicsek F. Wall stress as a possible mechanism for the development of transverse intimal tears in aortic dissections. Journal of medical engineering & technology. 1999; 23:127–134. [PubMed: 10561823]

Thubrikar MJ, Al-Soudi J, Robicsek F. Wall stress studies of abdominal aortic aneurysm in a clinical model. Annals of vascular surgery. 2001; 15:355–366. [PubMed: 11414088]

Tsai T, Evangelista A, Nienaber C, Myrmel T, Meinhardt G, Cooper J, Smith D, Suzuki T, Fattori R, Llovet A, et al. Partial thrombosis of the false lumen in patients with acute type B aortic dissection. New England Journal of Medicine. 2007; 357:349–359. [PubMed: 17652650]

Tsai T, Trimarchi S, Nienaber C. Acute aortic dissection: perspectives from the International Registry of Acute Aortic Dissection (IRAD). European Journal of Vascular and Endovascular Surgery. 2009; 37:149–159. [PubMed: 19097813]

Vasava P, Jalali P, Dabagh M, Kolari P. Finite element modelling of pulsatile blood flow in idealized model of human aortic arch: study of hypotension and hypertension. Computational and mathematical methods in medicine. 2012:2012.

Venkatasubramaniam A, Fagan M, Mehta T, Mylankal K, Ray B, Kuhan G, Chetter I, McCollum P. A comparative study of aortic wall stress using finite element analysis for ruptured and non-ruptured abdominal aortic aneurysms. European Journal of Vascular and Endovascular Surgery. 2004; 28:168–176. [PubMed: 15234698]

Wolak A, Gransar H, Thomson L, Friedman J, Hachamovitch R, Gutstein A, Shaw L, Polk D, Wong N, Saouaf R, et al. Aortic size assessment by noncontrast cardiac computed tomography: normal limits by age, gender, and body surface area. JACC: Cardiovascular Imaging. 2008; 1:200–209. [PubMed: 19356429]

Wuyts F, Vanhuyse V, Langewouters G, Decraemer W, Raman E, Buyle S. Elastic properties of human aortas in relation to age and atherosclerosis: a structural model. Physics in medicine and biology. 1995; 40:1577. [PubMed: 8532741]

Xie J, Zhou J, Fung Y. Bending of blood vessel wall: stress-strain laws of the intima-media and adventitial layers. Journal of biomechanical engineering. 1995; 117:136–145. [PubMed: 7609477]

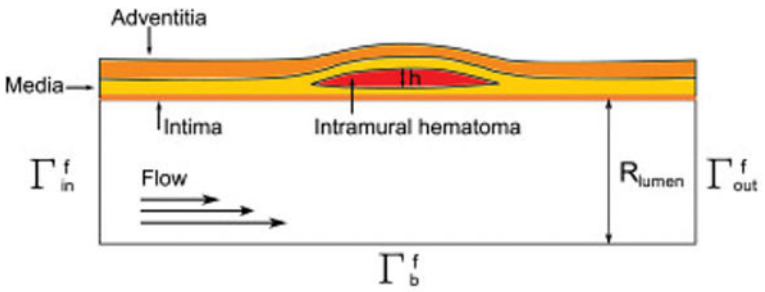

Figure 1.

Diagram of an idealized, axially symmetric model of an aorta. R_{lumen} denotes the lumen radius and h denotes the maximum IMH thickness.

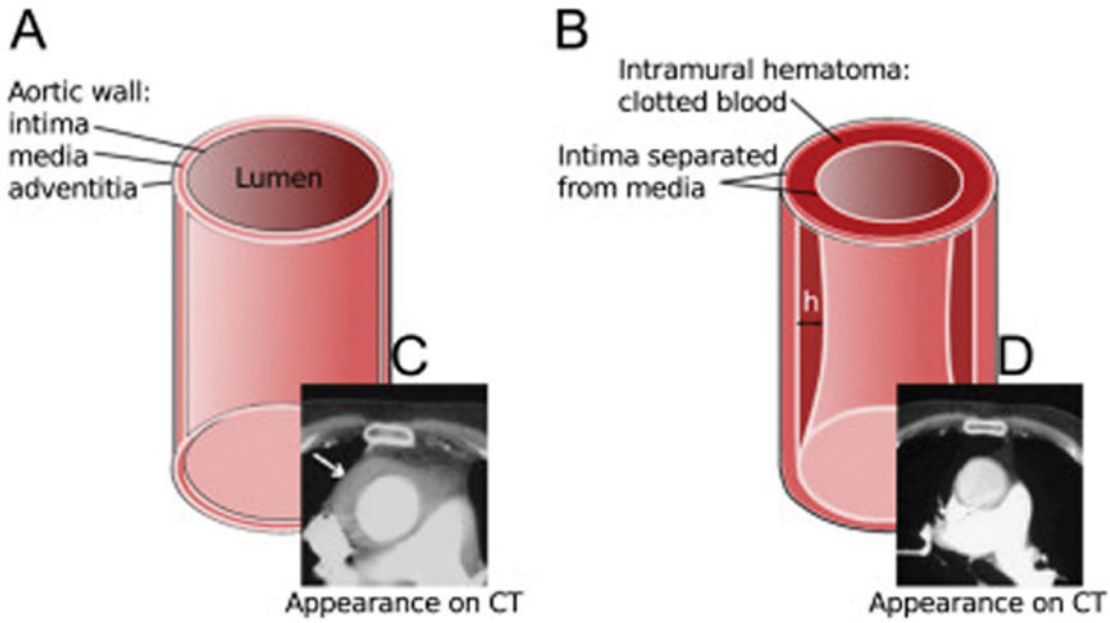

Figure 2.

A. Normal aorta. B. Aorta with IMH. C. CT image of normal aorta. D. CT image of aorta with IMH. CT images in panels C and D are taken from Masip (2004).

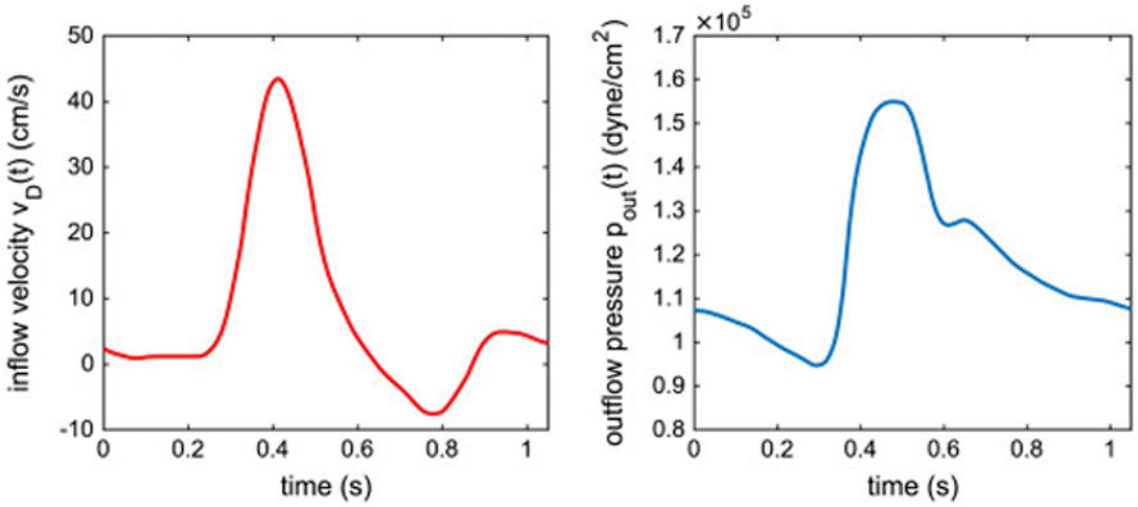

Figure 3.
Left: The velocity imposed at the inlet of the domain. Right: The pressure imposed at the outlet of the domain.

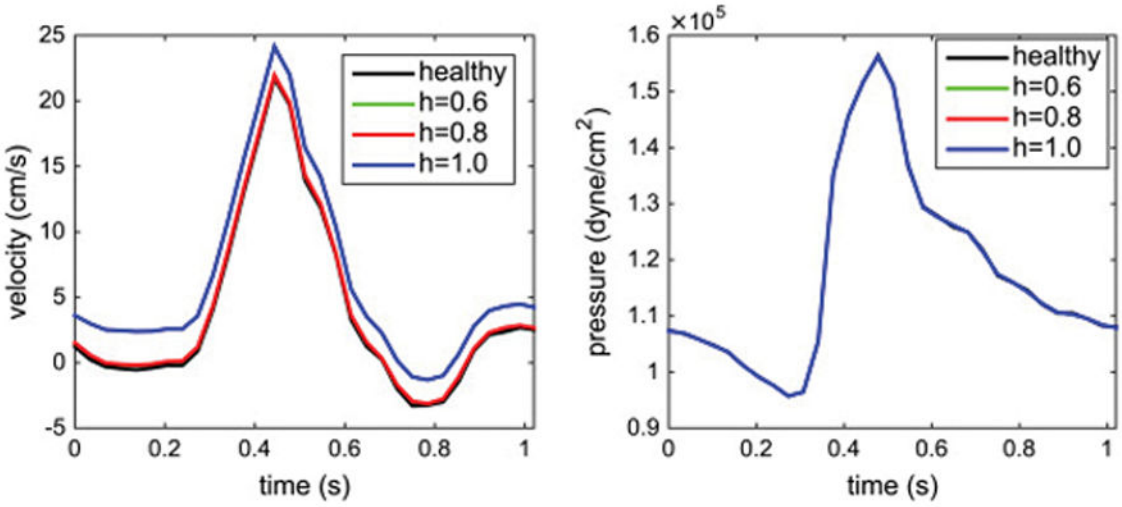

Figure 4.

Comparison of the velocity (left) and pressure (right) in the center of the lumen obtained in the case of a healthy aorta and diseased aortas with IMH thicknesses 0.6, 0.8 and 1.0 cm.

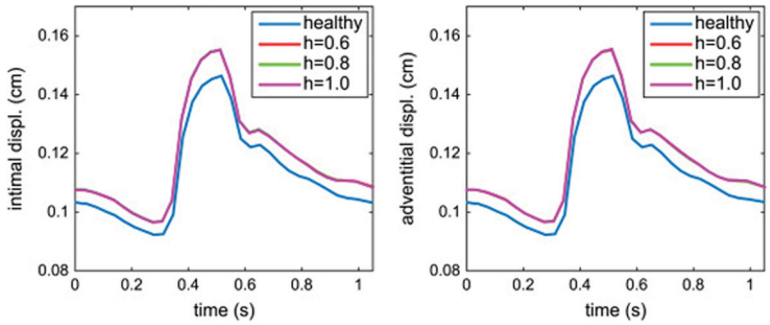

Figure 5.

Comparison of the displacement in the intima (left) and adventitia (right) at the center of the wall obtained in the case of a healthy aorta and diseased aortas with IMH thicknesses 0.6, 0.8 and 1.0 cm. The permeability of IMH is $10^{-10}\boldsymbol{I}$ cm^3 s/g.

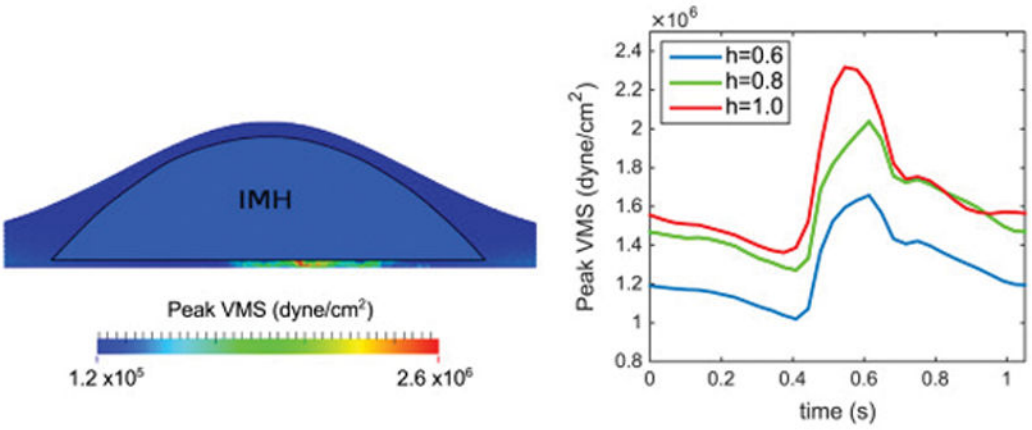

Figure 6.

Left: The Peak von Mises stress in the aorta with IMH of thickness 1.0 cm. Right: Comparison of the PWS in diseased aortas with IMH thicknesses 0.6, 0.8 and 1.0 cm. The PWS is slightly greater in aortas with thicker IMH.

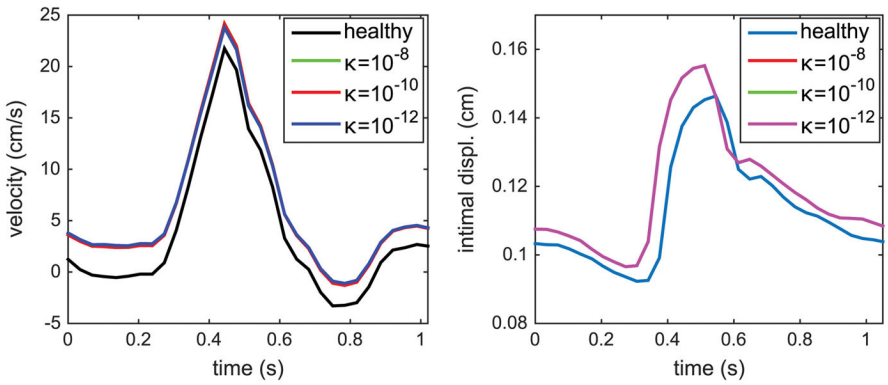

Figure 7.

Left: Comparison of the velocity in the center of the lumen obtained in the case of a healthy aorta and diseased aortas with IMH permeabilities 10^{-8}, 10^{-10} and $10^{-12}\boldsymbol{I}$ cm^3 s/g. Right: Comparison of the displacement in the intima at the center of the wall obtained in the case of a healthy aorta and diseased aortas. The thickness of IMH is 1.0 cm.

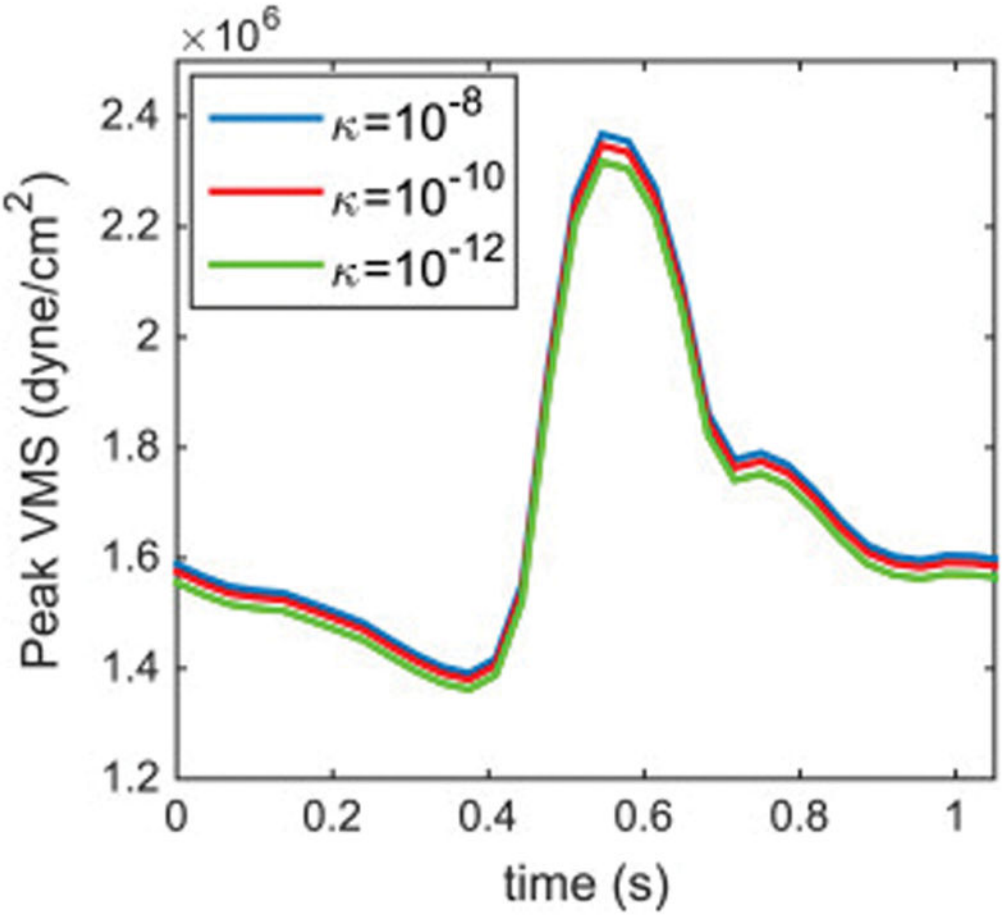

Figure 8.

Comparison of the PWS in diseased aortas with IMH permeabilities 10^{-8}, 10^{-10} and 10^{-12} ***I*** cm^3 s/g. The PWS is slightly greater in aortas with more permeable IMH.

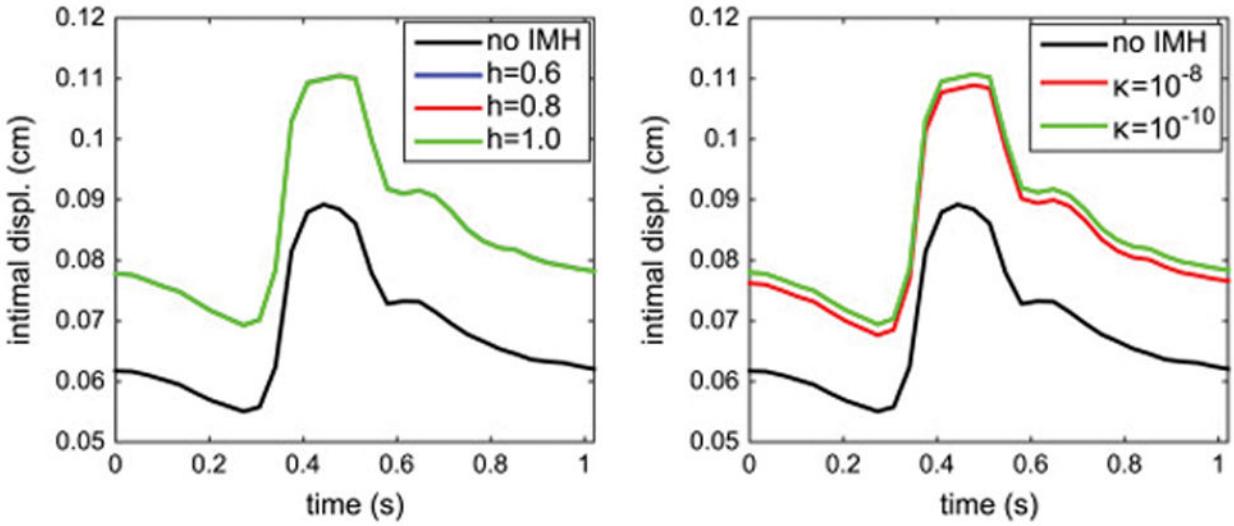

Figure 9.

Left: Comparison of the intimal displacement in old people without IMH and with IMHs being 0.6, 0.8 and 1.0 cm thick. Right: Comparison of the intimal displacement in older people without IMH and with IMH with permeabilities 10^{-8} and $10^{-10}\boldsymbol{I}$ cm^3 s/g.

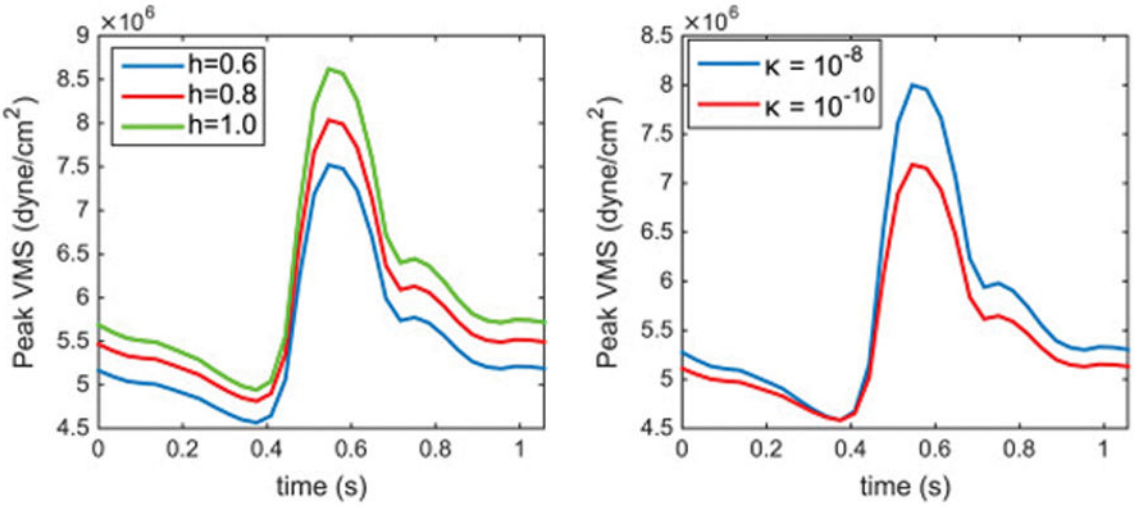

Figure 10.

Left: PWS in older people with IMHs of thicknesses 0.6, 0.8 and 1.0 cm and permeability $\boldsymbol{\kappa} = 10^{-10}\boldsymbol{I}$ cm^3 s/g. Right: PWS in older people with IMHs of permeabilities 10^{-8} and $10^{-10}\boldsymbol{I}$ cm^3 s/g and thickness 1.0 cm.